Stabilization of Electrocatalytic Metal Nanoparticles at Metal−Metal Oxide−Graphene Triple Junction Points

Rong Kou,[†,‡,#] Yuyan Shao,[†,‡] Donghai Mei,[†] Zimin Nie,[†] Donghai Wang,[†,¶] Chongmin Wang,[†] Vilayanur V Viswanathan,[†] Sehkyu Park,[†] Ilhan A. Aksay,[§] Yuehe Lin,[†] Yong Wang,*[,†,‖] and Jun Liu*[,†]
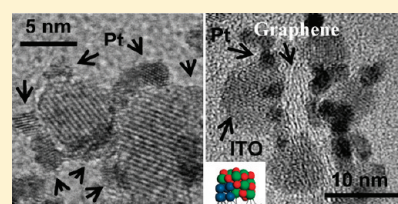
[†]Pacific Northwest National Laboratory, Richland, Washington 99352, United States

[§]Department of Chemical and Biological Engineering, Princeton University, Princeton, New Jersey 08544, United States

[‖]The Gene and Linda Voiland School of Chemical Engineering and Bioengineering, Washington State University, Pullman, Washington 99164, United States

S *Supporting Information*

ABSTRACT: Carbon-supported precious metal catalysts are widely used in heterogeneous catalysis and electrocatalysis, and enhancement of catalyst dispersion and stability by controlling the interfacial structure is highly desired. Here we report a new method to deposit metal oxides and metal nanoparticles on graphene and form stable metal−metal oxide−graphene triple junctions for electrocatalysis applications. We first synthesize indium tin oxide (ITO) nanocrystals directly on functionalized graphene sheets, forming an ITO−graphene hybrid. Platinum nanoparticles are then deposited, form-

ing a unique triple-junction structure (Pt−ITO−graphene). Our experimental work and periodic density functional theory (DFT) calculations show that the supported Pt nanoparticles are more stable at the Pt−ITO−graphene triple junctions. Furthermore, DFT calculations suggest that the defects and functional groups on graphene also play an important role in stabilizing the catalysts. These new catalyst materials were tested for oxygen reduction for potential applications in polymer electrolyte membrane fuel cells, and they exhibited greatly enhanced stability and activity.

INTRODUCTION

Precious metal nanoparticles (e.g., Pt, Au, Pd, and Rh) supported on carbon materials are one of the most widely used materials for heterogeneous and electrochemical catalysis. For these catalyst materials, the ability to control the dispersion and the durability of catalytic metal nanoparticles is essential to performance and economical feasibility. Herein, adjustments and optimizations of the interactions between the active metal phase and the support materials are the key factors to achieve this goal.[1,2] Recently, it has been proposed that hybrid materials, such as metal oxide−carbon complexes, should be used as the support for metal nanoparticles by synergistically combining the properties of both metal oxide and carbon materials.[3] Although there has already been a significant effort to accomplish this goal, controllable synthesis of these catalysts is difficult because of the complexity of these materials, preventing a clear understanding of the nature of interfacial interactions between metal nanoparticles and oxide−carbon materials.[4]

As one of the most widely used catalyst supports, carbon materials have a high surface area for the dispersion of metal nanoparticles, a porous structure for transferring reactants and products, and good electrical conductivity required for electrochemical reactions. However, the weak interaction between metal and carbon supports results in a severe sintering/agglomeration of catalytic metal nanoparticles and consequently decreases the active surface area, which leads to the degradation of

performance under long-term operations. The stability of the carbon material itself is also an important issue. For example, in polymer electrolyte membrane (PEM) fuel cells, carbon support corrosion ($C + 2H_2O \rightarrow CO_2 + 4H^+ + 4e^-$) is a serious problem with respect to the durability of electrocatalysts.[5−7] In the literature, many methods have been reported to address these problems, including using carbide, nitride, or metal oxides as catalyst supports.[3,8]

Metal oxides have also been widely used to support metal particles. These materials have higher stability than carbon in oxidizing environments.[9,10] Several conductive metal oxides have been investigated as catalyst supports in electrocatalysis with improved stability.[11−14] High surface area metal oxide nanoparticles are often desired to increase the metal dispersion and site density. However, high surface area metal oxides are also more difficult to stabilize and have a tendency to decrease the surface area due to coarsening in long-term operations.[15] More importantly, high surface area semiconducting metal oxides generally do not have sufficient electrical conductivity. This problem can be made worse by the porosity and disordering of the crystalline structure.[16,17] There have been several reports on loading metal oxides on carbon supports or coating carbon nanotubes with metal oxides to improve the activity and durability of the

catalysts.[18] The combination of metal oxides and carbon materials potentially allows the optimization of both the dispersion and the electrical conductivity.

In this study we used a functionalized graphene sheet (FGS), a newly developed two-dimensional (2-D) carbon material produced through thermal expansion and reduction of graphite oxide,[19] as the carbon support. Graphene in general has attracted wide attention because of its unique structure, high surface area, and high electrical conductivity. Graphene sheets have been used as the template to deposit metal catalysts for electrocatalysis[20,21] and as building blocks to form metal/graphene and metal oxide/ graphene supports for catalysts and battery applications.[22−25] In this work, we have developed a facile method to directly grow indium tin oxide (ITO) nanocrystals on functionalized graphene sheets to form ITO−graphene hybrids and studied their application as a Pt electrocatalyst support (in the rest of the paper, we will simply refer to "functionalized graphene sheets" as graphene or graphene sheets). Most carbon materials are disordered, and it is difficult to obtain direct information about the structures at the interfaces. The unique 2-D structure of graphene provides an ideal model to directly observe and closely study the structure and the morphology of the catalytic metal nanoparticles on support materials and to study the interaction between the catalytic metal and the hybrid support materials underneath. Our experimental results and density functional theory (DFT) modeling show that Pt nanoparticles are stabilized at ITO−graphene junctions forming a special Pt−ITO−graphene triple junction structure that has not been reported before. DFT calculations also provide important information on the role of the defects and functional groups of the graphene material on interfacial binding, a phenomenon seldom studied in the literature. These new catalyst materials were tested for oxygen reduction for potential application in PEM fuel cells, and they exhibited greatly enhanced performance, especially the durability. The concept of stabilizing metal catalysts at metal−metal oxide−graphene triple junctions might be extended to other catalytic applications.

■ METHODS

Synthesis of ITO Nanoparticles and ITO−Graphene Hybrids. First, graphene was dispersed in benzyl alcohol with a concentration of 0.0045 g/mL. Our graphene, due to the nature of its processing, contains topological defects, vacancies,[26] and oxygen functional groups (epoxy, hydroxy) with an approximate C/O ratio of 14.[19,27] As prepared, it contains approximately 80% single-sheet graphene along with stacked graphene (graphene stacks) as described previously.[19,27] Although it is possible to eliminate the stacked portion of the material by sedimentation methods, these stacks do not prevent us from accomplishing the goal of this study. To prepare ITO nanoparticles with a concentration of 10 wt % SnO_2, 0.2672 g of indium acetylacetonate [In(acac)$_3$] and 0.02729 g of tin(IV) *tert*-butoxide [Sn(OtBu)$_4$] were mixed with 20 mL of benzyl alcohol and stirred overnight before being transferred to an autoclave. To prepare the ITO−graphene hybrids, the designated amount of graphene/benzyl alcohol was added into the In(acac)$_3$ and Sn(OtBu)$_4$ solution and stirred overnight before it was transferred to an autoclave. Where not stated specifically in the paper, the autoclaves were heated to 200 °C and kept there for 17 h. The products were washed with ethanol and a large amount of chloroform, isolated by filtration, and finally dried in air.

Loading Pt Catalyst on Supporting Materials. A chemical reduction method was used to load 20 wt % Pt nanoparticles on different supporting materials.[28] First, 0.0525 g of H_2PtCl_5 was dissolved in 40 mL of ethylene glycol (EG), and the pH was adjusted to 12 with a 2 M

NaOH/EG solution. To load Pt on ITO−graphene hybrid, 0.1 g of ITO−graphene hybrid was added to the solution. The mixture was sonicated for 5 min and heated to 140 °C for 4 h. The products were washed with a large amount of water, isolated with filtration, and then dried in air. The same procedures were used to load Pt on other supports, including graphene, ITO, Vulcan XC-72 carbon black, and carbon nanotubes.

Material Characterization. The X-ray diffraction (XRD) characterization of the samples was performed with Cu Kα radiation at λ 1.54 Å on a Philips Xpert X-ray diffractometer. Transmission electron microscopy (TEM) characterization of the samples was performed with a JEOL TEM 2010 microscope equipped with an Oxford integrated scientific information system (ISIS). The operating voltage on the microscope was 200 keV. Nitrogen adsorption data were collected using Quantachrome autosorb automated gas sorption systems.

Electrochemical Characterization. The electrochemical characterization was carried out in a standard three-electrode cell using a Pt wire counter electrode and an Hg/Hg_2SO_4 reference electrode [0.69 V vs reversible hydrogen electrode (RHE)] at room temperature. Working electrodes were prepared by applying catalysts ink on prepolished glassy carbon electrodes (5 mm in diameter). The total loading of Pt was 3 μg. All electrode potentials are reported vs RHE.

Before measurements, working electrodes were first activated with cyclic voltammetry (CV) (0−1.1 V, 50 mV·s^{-1}) in a N_2-saturated 0.1 M $HClO_4$ solution until a steady CV was obtained. An oxygen reduction reaction (ORR) linear sweep voltammetry (LSV, positive-going potential scan, 5 mV·s^{-1}) was conducted in O_2-saturated 0.1 M $HClO_4$ on the rotating-disk electrode system (Pine Instruments). The ORR kinetic current values were obtained with the Koutecky−Levich equation.[8,29] The ORR current values measured in 0.1 M $HClO_4$ solution are quite different from those in 0.5 M H_2SO_4 solution, with the former being much higher than the latter.[30] Since many other studies conduct the ORR test in 0.1 M $HClO_4$,[8,31] we mostly report ORR current values in 0.1 M $HClO_4$ in this work. The durability tests were performed using the accelerated degradation test (ADT) protocol, which was specially designed to simulate PEM fuel cell working conditions in studying the durability of catalysts.[32] The CVs and oxygen-reduction polarization curves were recorded before and after 22 h of ADT testing, respectively.

The electrochemically active surface areas (ESAs) of Pt on each sample were calculated with Coulombic charges accumulated during hydrogen adsorption/desorption after correcting for the double-layer charging current from the CVs.[33] The ESA values measured in 0.5 M H_2SO_4 and in 0.1 M $HClO_4$ solution were similar.

Density Functional Theory Calculations. Periodic density functional theory (DFT) calculations were performed with the Vienna ab initio simulation package (VASP).[34,35] The model systems of graphene-supported ITO and Pt nanoparticles were described as an optimized ITO ($In_9Sn_1O_{15}$) cluster that was cut from an ITO bulk bixbyite structure and an optimized Pt cluster (6 Pt atoms) supported on the (6 × 6) supercell graphene sheet. The interaction energy (E_{int}) at 0 K between the cluster (ITO or Pt$_6$) and the graphene substrate was calculated as follows

$$E_{int} = E_{cluster + substrate} - (E_{cluster} + E_{substrate}) \qquad (1)$$

where $E_{cluster+substrate}$ is the total energy of the interacting system of the substrate and the supported cluster, $E_{substrate}$ is the total energy of the optimized bare graphene substrate slab, and $E_{cluster}$ is the energy of the optimized ITO or Pt$_6$ cluster in vacuum. With the definition given in eq 1, the more negative value of E_{int} indicates the stronger interaction between the supported cluster and the graphene substrate. In a similar way, we also calculated the interaction energy between the Pt$_6$ cluster and the ITO substrate. A periodic ITO(222) surface slab with nine atomic layers was used in the calculation. Since our graphene intrinsically has defects and oxygen-containing functional groups,[27] we also took into
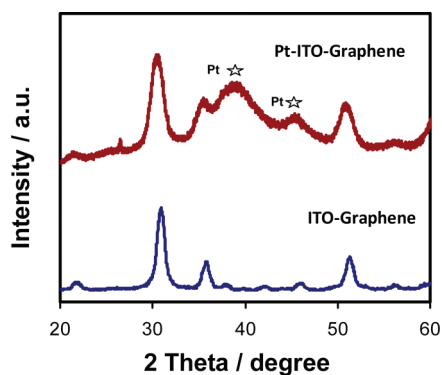
B

dx.doi.org/10.1021/ja107719u |*J. Am. Chem. Soc.* XXXX, XXX, 000–000

Figure 1. XRD patterns of ITO−graphene hybrid (75 wt % ITO) and Pt−ITO−graphene nanocomposite (20 wt % Pt).

consideration graphene with defects and/or oxygen functional groups. The details of the DFT calculations are given in the Supporting Information.

■ RESULTS AND DISCUSSION

Growth of ITO Nanoparticles on Graphene. While a systematic study on the growth of highly crystalline ITO nanoparticles in solution has been reported by Ba et al.,[36] who reported individual, isolated ITO nanocrystals with the bixbyite structure and with crystallite sizes of about 10−12 nm by a two-stage process, in our study, we strictly focus on the nucleation and growth of these particles on graphene. Similar to the observations of Ba et al.[36] and earlier findings on the formation of amorphous nuclei that later transform to a crystalline state during a multistage growth,[37] we show that a solid-state transformation to ITO also takes place at a later stage (17 h).

The XRD pattern of ITO (with 10 wt % SnO_2) grown on graphene after 17 h of reaction time is shown in the lower part of Figure 1. Intense reflection peaks corresponding to the highly crystalline cubic bixbyite structure of In_2O_3 (ICDD PDF No. 6-416) are observed. Since peaks corresponding to crystalline SnO_2 phase are not observed, we conclude that a solid solution rather than a mixture of indium oxide and tin oxide is produced.[38] Energy dispersive X-ray analysis spectroscopy of the ITO−graphene hybrid showed the presence of Sn (∼10%). The average crystallite size of ITO after a reaction of 17 h is estimated to be around 12 nm using the Scherrer equation.

The TEM investigation of the ITO particle growth on graphene showed the formation of amorphous nanoparticles after 1 h followed by a transformation to highly crystalline ITO nanoparticles after 17 h (Figure S1, Supporting Information). Figure 2a shows a TEM image of ITO−graphene hybrids (all ITO−graphene hybrids contain 75 wt % ITO and 25 wt % graphene unless otherwise stated). A uniform distribution of ITO particles ∼10 nm in diameter, consistent with the average particle size estimated by XRD analysis, is observed. Thus, the crystallite size determined by the Scherrer method corresponds to the nanoparticle size itself, suggesting that the individual particles must be mainly single crystals of ITO. This conjecture is supported by the lattice fringe images of Figure 2b. The spacings of the lattice fringes in two adjacent particles, which appear to be fused together, are 0.29 and 0.18 nm, corresponding to the d-spacings of the ITO crystalline planes of (222) and (440), respectively. Since the selected area electron diffraction (SAED)
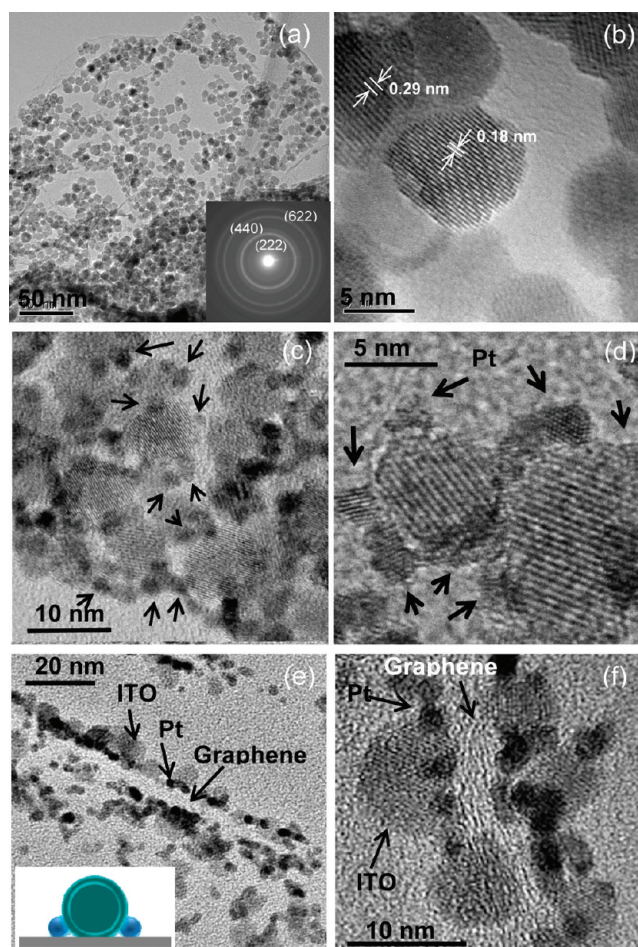

Figure 2. TEM images of ITO nanoparticles on graphene sheets (a, b), Pt−ITO−graphene (c, d), and the cross section TEM images of Pt−ITO−graphene (e, f). Inset: The schematic structure of Pt−ITO−graphene nanocomposite. ITO content in ITO−graphene composite is 75 wt % and Pt content in Pt−ITO−graphene is 20 wt %.

shows a polycrystalline texture, the ITO nanoparticles on graphene must be randomly oriented in contrast to the high degree of orientational order observed by Ba et al.[36] in the early stages of growth.

We used these highly crystalline ITO nanoparticles on graphene (ITO−graphene, 17 h reaction time) as the Pt catalyst support for our studies as detailed below.

Pt−ITO−Graphene Nanocomposites. The XRD pattern of the Pt−ITO−graphene nanocomposite in Figure 1 shows peaks indexing to Pt, indicating the formation of Pt particles smaller than the ITO particles, as evidenced by the broader peaks in comparison to those of ITO. The XRD data are supported by the high-resolution TEM image of Figure 2c, which shows that while the ITO nanoparticles are ∼10 nm in diameter, the Pt nanoparticles are ∼2 nm in diameter. Similar to the uniform distribution of ITO particles, the Pt nanoparticles are also highly dispersed on the ITO−graphene hybrid without agglomeration. In contrast, the Pt nanoparticles on graphene show a high degree of aggregation (Figure S6, Supporting Information) with the Pt particle size ranging from 2 nm to several tens of nanometers. This indicates that the ITO nanoparticles on graphene help disperse Pt nanoparticles. Figure 2c also shows that the majority of the Pt nanoparticles are on the surface or at the grain boundaries

of the ITO nanoparticles (marked with arrows). Figure 2d shows that the crystalline Pt nanoparticles are formed on the surface of ITO particles. Cross-section TEM images (Figure 2e,f) further reveal the exact location of Pt and ITO nanoparticles in the Pt−ITO−graphene nanocomposite. In the low-magnification cross-section image (Figure 2e), the graphene stacks are observed as a narrow band, and both sides of graphene stacks are coated with ITO and Pt nanoparticles. The graphene layers are clearly observed in the high-resolution image of Figure 2f. As we discussed in a previous publication,[39] the TEM observation is biased toward the stacked structure of graphene, because a single layer of graphene sheet is difficult, if not impossible, to image in the embedded cross-section TEM sample. Furthermore, we could not rule out the possibility of some degree of restacking of single-layer graphene into graphene stacks during processing. Therefore, the final graphene material most likely contains a mixture of single-layer graphene and graphene stacks. A unique observation from these TEM images is that while the graphene stacks (marked) are coated by one layer of ITO nanoparticles or islands of fused ITO nanoparticles, Pt nanoparticles are deposited at the interface between the ITO and graphene, as schematically illustrated in Figure 2e (Inset). Figure 2f reveals the location of Pt nanoparticles at junctions between ITO and graphene (Pt nanoparticles bonded with both graphene and ITO at the corner to form triple junctions) instead of on the graphene only or on the ITO surface only. Thus, combining the face-on and the cross-sectional images in Figure 2, we conclude that Pt nanoparticles are preferentially located at the junctions between ITO and graphene, forming the unique triple junction structure.

In a previous study, we reported that Pt nanoparticles are more likely to bond to the graphene surface through defects and functional groups (e.g., hydroxyl, epoxy).[20] The strong interaction between Pt and defects/functional groups improved the activity and stability of Pt nanoparticles on graphene.[20] Metal oxide nanoparticles are also known to have a strong interaction with Pt nanoparticles.[11,14] Therefore, when Pt nanoparticles are deposited on the ITO−graphene hybrid, whether the Pt nanoparticles bond with ITO, with graphene, or both will be affected by a balance of Pt−ITO and Pt−graphene interaction energies.

DFT Calculations. To better understand the preferential bonding of Pt nanoparticle with both ITO nanoparticle and graphene support at the triple junction points, DFT calculations were conducted. According to previous experimental[27] and theoretical[40] studies, a 5−8−5 defect is considered to be the most stable defect in our graphene[27] while the functional groups are the hydroxyls (−OH) and epoxies (C−O−).[27,41] The interaction energies (E_{int}) of adsorbed clusters (Pt, ITO, ITO−Pt) on four different substrates: perfect graphene, graphene with 5−8−5 defect, graphene with 5−8−5 defect and epoxy, and graphene with 5−8−5 defect and hydroxyl (see Figure 3 and Figure S2−S4 in Supporting Information), were determined using periodic DFT calculations. The results including the Pt_6 cluster on the ITO(222) substrate are given in Table 1. The enhanced interaction (ΔE_{int}) for Pt−ITO−graphene with triple junction configuration was calculated using eq 2:

$$\Delta E_{int} = E_{int}(ITO–Pt_6) - [E_{int}(Pt_6) + E_{int}(ITO)] \quad (2)$$

where $E_{int}(ITO−Pt_6)$ is the calculated interaction energy between supported cluster ($ITO−Pt_6$) and graphene substrate (with triple junction configuration), $E_{int}(Pt_6)$ is the calculated interaction energy between isolated Pt_6 cluster and graphene
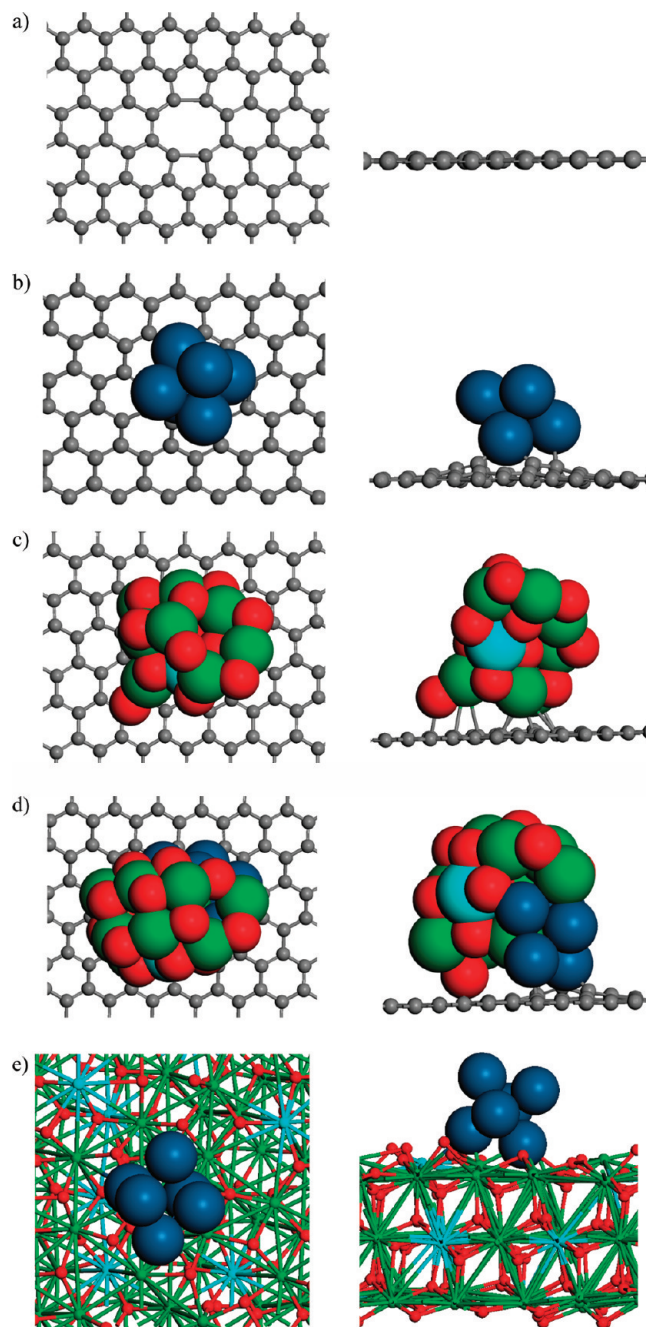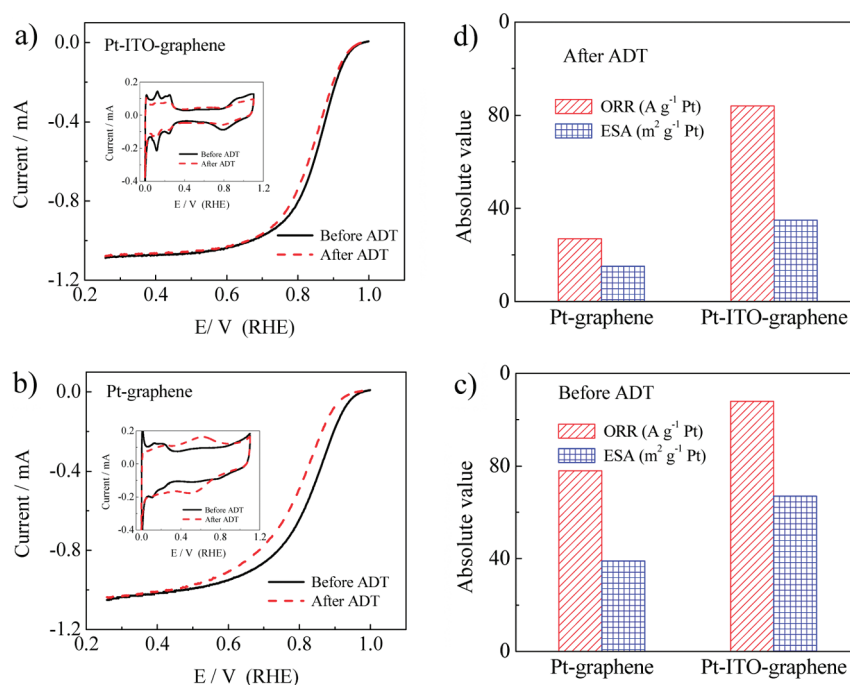

Figure 3. The top views (left) and side views (right) of graphene with 5−8−5 defect (a), Pt_6 cluster on graphene with 5−8−5 defect (b), ITO ($In_9Sn_1O_{15}$) cluster on graphene with 5−8−5 defect (c), Pt_6−ITO−graphene triple junction structure (d), and Pt_6 cluster on ITO(222) surface (e). Graphene sheet is displayed as gray balls for clarity; indium atoms are in green, oxygen atoms are in red, platinum atoms are in dark blue, and tin atoms are in light blue.

substrate, and $E_{int}(ITO)$ is the calculated interaction energy between isolated ITO cluster and graphene substrate. The more negative value of ΔE_{int} indicates that the formation of Pt−ITO−graphene triple junctions is more thermodynamically favorable instead of isolated Pt and ITO clusters on the graphene sheets. As shown in Table 1, on all the four different graphene substrates, the formation of Pt−ITO−graphene triple junction structure is preferred (ΔE_{int} <0), and on the 5−8−5 defect

Table 1. DFT Calculated Interaction Energies (E_{int}, eV) of Adsorbed Clusters on Graphene and ITO Substrate Surfaces[a]

adsorbed cluster	perfect graphene	graphene with 5−8−5 defect	graphene with 5−8−5 defect and epoxy	graphene with 5−8−5 defect and hydroxyl	ITO(222)
Pt_6	−2.64	−9.38	−9.98	−7.28	−5.56
ITO ($In_9Sn_1O_{15}$)	−1.36	−1.04	−1.46	−3.12	−
$ITO-Pt_6$	−9.58	−20.64	−14.74	−13.94	−
ΔE_{int}	−5.58	−10.22	−3.30	−3.45	

[a] $\Delta E_{int} = E_{int}(ITO-Pt_6) - [E_{int}(Pt_6) + E_{int}(ITO)]$ is the enhanced interaction for Pt−ITO−graphene with triple junction structure.

Figure 4. Linear sweep voltammetry polarization curves of oxygen reduction on Pt−ITO−graphene (a) and Pt−graphene (b) in O_2-saturated 0.1 M $HClO_4$ (5 mV·s^{-1}, 1600 rpm). Inset: Cyclic voltammograms on Pt−ITO−graphene and Pt−graphene in N_2-saturated 0.1 M $HClO_4$ (50 mV·s^{-1}). (c, d) Electrochemically active surface area (ESA) and oxygen reduction reaction (ORR) kinetic currents before and after 22 h accelerated degradation test (ADT).

graphene substrate, the Pt−ITO−graphene triple junction structure is highly stable (the highest absolute value of ΔE_{int}). For the case of isolated Pt_6 cluster, the $E_{int}(Pt_6)$ on the graphene with 5−8−5 defects or functional groups are much larger than that on perfect graphene, indicating the enhanced stabilization of Pt_6 cluster at defect and functional groups sites on graphene sheets. This is consistent with our previous study.[20] On the other hand, the calculated interaction energy of the Pt_6 cluster on the most stable ITO(222) surface is −5.56 eV, which is lower (in absolute value) than any $E_{int}(ITO-Pt_6)$ on all four kinds of graphene substrates, suggesting that supported Pt clusters prefer to bond at the interface between ITO and graphene, forming the triple junction structure instead of bonding onto ITO particles only. Thus, the DFT calculation results are consistent with the TEM observations that Pt nanoparticles favor the ITO−graphene interface, forming triple junctions. The strong interaction between Pt nanoparticles and the ITO−graphene interface results in a unique Pt−ITO−graphene triple junction structure that eventually determines the dispersion of the active metal Pt phase.

We expect that the enhanced stabilization of Pt nanoparticles at the ITO−graphene junctions should improve catalytic activity and the stability of Pt−ITO−graphene. In the following section, the electrochemical test results of oxygen reduction on Pt−

ITO−graphene electrocatalysts (for potential application in PEM fuel cells) are presented to support this view.

Electrochemical Tests. Since the activity and stability of oxygen-reduction electrocatalysts are the key challenges for PEM fuel cell commercialization, we studied the electrochemical performance of the Pt−ITO−graphene nanocomposite as an electrocatalyst for oxygen reduction to demonstrate the enhanced performance of Pt stabilization at the junctions. Figure 4 shows the electrochemical test results.

The catalytic activity of Pt−ITO−graphene, measured with oxygen reduction linear sweep voltammetry (LSV) curves obtained before and after ADT, showed only a 14 mV degradation in half-wave potential (Figure 4a); in contrast, the corresponding change for Pt−graphene was as high as 40 mV (Figure 4b). The ORR kinetic mass activities before and after ADT are shown in Figure 4c,d. The initial mass activities (before ADT) of Pt−ITO−graphene and Pt−graphene are 108 and 78 A·g^{-1} Pt, respectively, which are, after ADT, decreased to 84 A·g^{-1} Pt (77.8% retention) and 26 A·g^{-1} Pt (33.3% retention), respectively, indicating significantly improved stability and activity on Pt−ITO−graphene.

ESAs of Pt before and after ADT (from the CVs of Figure 4a,b insets) were calculated to be 67 and 40 m^2·g^{-1} Pt for Pt−ITO−graphene and Pt−graphene, respectively (Figure 4c,d);

E

dx.doi.org/10.1021/ja107719u |*J. Am. Chem. Soc.* XXXX, XXX, 000−000

after ADT, the ESAs decreased to 36.4 $m^2 \cdot g^{-1}$ Pt (54.3% retention) and 15.2 $m^2 \cdot g^{-1}$ Pt (38% retention), respectively. As expected, these ESA results are in good agreement with the measured ORR activity results.

The degradation of electrocatalysts can also be seen from post-mortem TEM analysis. The TEM images of electrocatalysts after the durability tests show significant agglomeration of Pt nanoparticles in Pt–graphene but much less Pt agglomeration in Pt–ITO–graphene (Figure S6, Supporting Information), confirming the importance of stabilization of Pt nanoparticles in Pt–ITO–graphene nanocomposite. This is important for practical applications in PEM fuel cells as the agglomeration of Pt nanoparticles is one of the main reasons for the degradation of PEM fuel cell electrocatalysts.[5,7]

In addition to showing the role of Pt stabilization on PEM fuel cell performance, we have also compared the performance of Pt–ITO–graphene with other widely used carbon-supported electrocatalysts, such as Pt–carbon nanotube (Pt–CNT), Pt–Vulcan carbon black (Pt–C), and commercial ETek Pt catalyst. The results show that Pt–ITO–graphene has both the highest durability and the highest activity among all the materials studied in this work (Figure S7, Supporting Information), indicating a promising electrocatalytic material for oxygen reduction in PEM fuel cells. Further, we have also found that, with ITO coating, graphene substrate is very resistant to oxidation (Figure S8, Supporting Information), which should also contribute to the excellent durability of Pt–ITO–graphene.

CONCLUSION

In this study, we synthesized ITO–graphene hybrid material and loaded catalytic metal Pt nanoparticles on the hybrid material. We are able to produce a unique structure of Pt–ITO–graphene triple junctions and study the structure–property relationship. DFT calculations indicate that the deposition of Pt nanoparticles is thermodynamically favored and stabilized at the metal oxide–graphene junctions. The defects and functional groups on graphene also help improve the stability of the catalysts. Pt–ITO–graphene nanocomposites were investigated as electrocatalysts for oxygen reduction for potential application in PEM fuel cells. The ITO–graphene hybrid substrates possess the desired properties of the metal oxide and graphene sheets. The graphene sheets function as a scaffold that provides the high surface area and greatly increases the electrical conductivity. The ITO nanoparticles are evenly dispersed and protect graphene from corrosion, improving the durability of the substrate. The unique triple junction structure in the nanocomposite with a high surface area, good metal dispersion, and good electrical conductivity make such materials suitable for PEM fuel cell applications. The electrochemical tests show that the performance of Pt supported on ITO–graphene hybrid substrates, especially the durability, is not only better than that of Pt supported on graphene sheets but also better than the widely used Pt electrocatalysts supported with carbon materials (e.g., Vulcan carbon XC72 and carbon nanotubes). This study provides a new understanding of the nature of the interactions in complex metal catalyst, metal oxide, and carbon materials and may be extended to study the structure and properties of other carbon-supported catalyst materials.

ASSOCIATED CONTENT

S **Supporting Information.** All experimental procedures and DFT calculation details; TEM images of ITO grown on graphene sheets during different reaction times; modeling structures of Pt_6 cluster on graphene with/without defects and functional groups; more TEM images of Pt–ITO–graphene and Pt–graphene before and after the electrochemical durability test; a comparison of the activity and durability of Pt–ITO–graphene, Pt–graphene, Pt–C, Pt–CNT, and ETek electrocatalysts; and complete authorship listing for ref 6. This material is available free of charge via the Internet at http://pubs.acs.org.

AUTHOR INFORMATION

Corresponding Author
yong.wang@pnl.gov; jun.liu@pnl.gov

Present Addresses
#EC Power, LLC State College, PA 16801.
¶The Pennsylvania State University, Department of Mechanical and Nuclear Engineering, University Park, PA 16802.

Author Contributions
‡These authors contributed equally.

REFERENCES

(1) Yin, S. B.; Mu, S. C.; Lv, H. F.; Cheng, N. A. C.; Pan, M.; Fu, Z. Y. *Appl. Catal. B-Environ.* **2010**, *93*, 233–240.

(2) He, P.; Liu, M.; Luo, J. L.; Sanger, A. R.; Chuang, K. T. *J. Electrochem. Soc.* **2002**, *149*, A808–A814.

(3) Shao, Y. Y.; Liu, J.; Wang, Y.; Lin, Y. H. *J. Mater. Chem.* **2009**, *19*, 46–59.

(4) Kwak, J. H.; Hu, J. Z.; Mei, D.; Yi, C. W.; Kim, D. H.; Peden, C. H. F.; Allard, L. F.; Szanyi, J. *Science* **2009**, *325*, 1670–1673.

(5) Shao, Y. Y.; Yin, G. P.; Gao, Y. Z. *J. Power Sources* **2007**, *171*, 558–566.

(6) Borup, R. *Chem. Rev.* **2007**, *107*, 3904–3951.

(7) Shao-Horn, Y.; Sheng, W.; Chen, S.; Ferreira, P.; Holby, E.; Morgan, D. *Top. Catal.* **2007**, *46*, 285–305.

(8) Gasteiger, H. A.; Kocha, S. S.; Sompalli, B.; Wagner, F. T. *Appl. Catal. B-Environ.* **2005**, *56*, 9–35.

(9) Matsui, T.; Fujiwara, K.; Okanishi, T.; Kikuchi, R.; Takeguchi, T.; Eguchi, K. *J Power Sources* **2006**, *155*, 152–156.

(10) Zheng, N. F.; Stucky, G. D. *J. Am. Chem. Soc.* **2006**, *128*, 14278–14280.

(11) Park, K. W.; Seol, K. S. *Electrochem. Commun.* **2007**, *9*, 2256–2260.

(12) Formo, E.; Lee, E.; Campbell, D.; Xia, Y. N. *Nano Lett.* **2008**, *8*, 668–672.

(13) Chhina, H.; Campbell, S.; Kesler, O. *J. Power Sources* **2006**, *161*, 893–900.

(14) Huang, S. Y.; Ganesan, P.; Park, S.; Popov, B. N. *J. Am. Chem. Soc.* **2009**, *131*, 13898–13899.

(15) Buhler, G.; Tholmann, D.; Feldmann, C. *Adv. Mater.* **2007**, *19*, 2224–2227.

F

dx.doi.org/10.1021/ja107719u |*J. Am. Chem. Soc.* XXXX, XXX, 000–000

(16) Fattakhova-Rohlfing, D.; Brezesinski, T.; Smarsly, B.; Rathousky, J. *Superlattices Microstruct.* **2008**, *44*, 686–692.

(17) Biswas, P. K.; De, A.; Pramanik, N. C.; Chakraborty, P. K.; Ortner, K.; Hock, V.; Korder, S. *Mater. Lett.* **2003**, *57*, 2326–2332.

(18) Shannnigarn, S.; Gedanken, A. *Small* **2007**, *3*, 1189–1193.

(19) McAllister, M. J.; Li, J. L.; Adamson, D. H.; Schniepp, H. C.; Abdala, A. A.; Liu, J.; Herrera-Alonso, M.; Milius, D. L.; Car, R.; Prud'homme, R. K.; Aksay, I. A. *Chem. Mater.* **2007**, *19*, 4396–4404.

(20) Kou, R.; Shao, Y. Y.; Wang, D. H.; Engelhard, M. H.; Kwak, J. H.; Wang, J.; Viswanathan, V. V.; Wang, C. M.; Lin, Y. H.; Wang, Y.; Aksay, I. A.; Liu, J. *Electrochem. Commun.* **2009**, *11*, 954–957.

(21) Seger, B.; Kamat, P. V. *J. Phys. Chem. C* **2009**, *113*, 7990–7995.

(22) Wang, D. H.; Choi, D. W.; Li, J.; Yang, Z. G.; Nie, Z. M.; Kou, R.; Hu, D. H.; Wang, C. M.; Saraf, L. V.; Zhang, J. G.; Aksay, I. A.; Liu, J. *ACS Nano* **2009**, *3*, 907–914.

(23) Paek, S. M.; Yoo, E.; Honma, I. *Nano Lett.* **2009**, *9*, 72–75.

(24) Goncalves, G.; Marques, P.; Granadeiro, C. M.; Nogueira, H. I. S.; Singh, M. K.; Gracio, J. *Chem. Mater.* **2009**, *21*, 4796–4802.

(25) Xu, C.; Wang, X.; Zhu, J. W. *J. Phys. Chem. C* **2008**, *112*, 19841–19845.

(26) Kudin, K. N.; Ozbas, B.; Schniepp, H. C.; Prud'homme, R. K.; Aksay, I. A.; Car, R. *Nano Lett.* **2008**, *8*, 36–41.

(27) Schniepp, H. C.; Li, J. L.; McAllister, M. J.; Sai, H.; Herrera-Alonso, M.; Adamson, D. H.; Prud'homme, R. K.; Car, R.; Saville, D. A.; Aksay, I. A. *J. Phys. Chem. B* **2006**, *110*, 8535–8539.

(28) Shao, Y.; Zhang, S.; Kou, R.; Wang, X.; Wang, C.; Dai, S.; Viswanathan, V.; Liu, J.; Wang, Y.; Lin, Y. *J. Power Sources* **2010**, *195*, 1805–1811.

(29) Mayrhofer, K. J. J.; Strmcnik, D.; Blizanac, B. B.; Stamenkovic, V.; Arenz, M.; Markovic, N. M. *Electrochim. Acta* **2008**, *53*, 3181–3188.

(30) Wang, J. X.; Markovic, N. M.; Adzic, R. R. *J. Phys. Chem. B* **2004**, *108*, 4127–4133.

(31) Paulus, U. A.; Schmidt, T. J.; Gasteiger, H. A.; Behm, R. J. *J. Electroanal. Chem.* **2001**, *495*, 134–145.

(32) Shao, Y. Y.; Kou, R.; Wang, J.; Viswanathan, V. V.; Kwak, J. H.; Liu, J.; Wang, Y.; Lin, Y. H. *J. Power Sources* **2008**, *185*, 280–286.

(33) Shao, Y. Y.; Yin, G. P.; Wang, J. J.; Gao, Y. Z.; Shi, P. F. *J. Electrochem. Soc.* **2006**, *153*, A1261–A1265.

(34) Kresse, G.; Furthmuller, J. *Phys. Rev. B* **1996**, *54*, 11169–11186.

(35) Kresse, G.; Furthmuller, J. *Comput. Mater. Sci.* **1996**, *6*, 15–50.

(36) Ba, J.; Feldhoff, A.; Fattakhova-Rohlfing, D.; Wark, M.; Antonietti, M.; Niederberger, M. *Small* **2007**, *3*, 310–317.

(37) Xu, G. F.; Yao, N.; Aksay, I. A.; Groves, J. T. *J. Am. Chem. Soc.* **1998**, *120*, 11977–11985.

(38) Ba, J. H.; Fattakhova-Rohlfing, D.; Feldhoff, A.; Brezesinski, T.; Djerdj, I.; Wark, M.; Niederberger, M. *Chem. Mater.* **2006**, *18*, 2848–2854.

(39) Wang, D. H.; Kou, R.; Choi, D.; Yang, Z. G.; Nie, Z. M.; Li, J.; Saraf, L. V.; Hu, D. H.; Zhang, J. G.; Graff, G. L.; Liu, J.; Pope, M. A.; Aksay, I. A. *ACS Nano* **2010**, *4*, 1587–1595.

(40) Lee, G. D.; Wang, C. Z.; Yoon, E.; Hwang, N. M.; Kim, D. Y.; Ho, K. M. *Phys. Rev. Lett.* **2005**, *95*, 205501.

(41) Dreyer, D. R.; Park, S.; Bielawski, C. W.; Ruoff, R. S. *Chem. Soc. Rev.* **2010**, *39*, 228–240.